EEET ECOLOGICAL ENGINEERING & ENVIRONMENTAL TECHNOLOGY

Ecological Engineering & Environmental Technology, 2026, 27(1), 336–349
https://doi.org/10.12912/27197050/215789
ISSN 2719–7050, License CC-BY 4.0

Received: 2025.11.22
Accepted: 2025.12.18
Published: 2026.01.01

Assessment of waterlogging susceptibility in oil palm plantation using data-driven predictive modelling

Yan Sukmawan[1,2], Ahmad Juneadi[3], Hariyadi[3], Supijatno[3], Lilik Budi Prasetyo[4*], Arif Kurnia Wijayanto[4]

[1] Program of Agronomy and Horticulture, Graduate School, Faculty of Agriculture, IPB University, Jl. Meranti Kampus IPB Dramaga, Bogor 16680, Indonesia
[2] Estate Crop Department, Politeknik Negeri Lampung, Jl. Soekarno-Hatta No. 10, Bandar Lampung 35144, Indonesia
[3] Department of Agronomy and Horticulture, Faculty of Agriculture, IPB University, Jl. Meranti Kampus IPB Dramaga, Bogor 16680, Indonesia
[4] Department of Forest Resources Conservation and Ecotourism, Faculty of Forestry and Environment, IPB University, Jl. Ulin Lingkar Akademik Kampus IPB Darmaga, Bogor 16680, Indonesia
* Corresponding author's e-mail: lbprastdp@apps.ipb.ac.id

ABSTRACT

Accurate assessment of waterlogging susceptibility is important for maintaining productivity and ecological stability in oil palm plantations, particularly in the face of increasing climate-driven rainfall variability. Direct field measurements of plant and soil water status provide reliable information but are labor-intensive and impractical for repeated monitoring at plantation scale. This study proposes a data-driven predictive modelling framework to assess waterlogging susceptibility in oil palm plantations using UAV-derived multispectral information. Field and aerial data were collected at the Oil Palm Teaching Farm, IPB University, Indonesia, during four seasonal observation periods (July 2024, October 2024, January 2025, and April 2025). Multispectral orthomosaics were generated, and twelve vegetation indices were extracted at the individual palm canopy level. Soil moisture, leaf water content, and leaf greenness were measured in the field and used as reference data to develop predictive models based on Random Forest Regression, Partial Least Squares Regression, and Support Vector Regression. The modelling results showed that Partial Least Squares Regression provided the best performance for soil moisture estimation ($R^2 = 0.61$), while Random Forest Regression achieved high accuracy in predicting leaf greenness ($R^2 = 0.83$). In contrast, all models exhibited limited performance in estimating leaf water content ($R^2 < 0.50$), indicating low sensitivity of multispectral vegetation indices to variations in oil palm leaf water status. Consequently, waterlogging susceptibility mapping was conducted based on the integrated spatial patterns of predicted soil moisture and leaf greenness. The resulting susceptibility maps successfully identified palms vulnerable to prolonged waterlogging and associated productivity decline. These findings demonstrate that data-driven predictive modelling using UAV multispectral data can provide a practical and scalable approach for spatially explicit assessment of waterlogging susceptibility in oil palm plantations, supporting informed decision-making in precision and environmentally sustainable plantation management.

Keywords: climate change, machine learning, multispectral imagery, oil palm, precision agriculture, unmanned aerial vehicle, waterlogging susceptibility.

INTRODUCTION

Oil palm (*Elaeis guineensis* Jacq.) is a major source of vegetable oil, accounting for 40% of global vegetable oil production, despite occupying only 5% of the land used for vegetable oil production (Jackson et al., 2019). The high productivity and economic value of oil palm enable the sustainable fulfillment of future oil demands (Murphy et al., 2021). To ensure

sustainability, the oil palm industry is focusing on increasing yields, improving oil quality, and enhancing climate adaptation through germplasm exploitation and biotechnology (Malike et al., 2024). However, oil palm productivity is heavily influenced by climate factors, with water availability being the cornerstone of sustainable production (Rauf, 2025). Global climate change exacerbates this dependence, driving increased volatility in crude palm oil (CPO) yields through changes in precipitation patterns and other factors. Two unfavorable conditions, water deficit and excess, disrupt the balance of physiological processes in crops. Water deficit causes stomatal closure, which reduces photosynthesis and disrupts nutrient uptake, leading to decreased growth (Neto et al., 2021) and reduced fruit bunch production (Khor et al., 2021). Conversely, prolonged waterlogging or flooding causes root hypoxia, which inhibits root respiration, triggers root rot, and ultimately reduces crop productivity (Abubakar et al., 2021). Therefore, effective and timely monitoring of plant water status is crucial for the proper management of water stress, allowing interventions in plantation management to maintain the yield.

Conventional methods for monitoring crop water status, such as direct soil sampling or leaf water content measurements, are primarily point-based, labor-intensive, and impractical for large-scale plantations (Jha et al., 2025). Remote sensing technology offers a transformative solution for achieving efficiency and effectiveness. By measuring the electromagnetic radiation reflected by plant tissues, remote sensing enables non-destructive and spatial assessments of crop status. Unmanned aerial vehicle (UAV) are further revolutionizing this field by bridging the gap between lower spatial resolution satellite imagery and the limitations of ground-based agronomic surveys. UAV equipped with multispectral sensors provide data at high spatial and temporal resolutions, enabling precise monitoring of within-field variability. This capability is particularly important for perennial crops, such as oil palms, where even subtle changes in canopy reflectance can be observed.

Vegetation indices (VI) obtained from remote sensing platforms have emerged as powerful non-destructive proxies for monitoring plant and soil biophysical parameters (Falcioni et al., 2023; Zeng et al., 2022). Previous studies have demonstrated the effectiveness of combining spectral indices with machine learning algorithms to achieve high-precision estimates. For leaf water content (LWC) estimation using hyperspectral data, techniques such as competitive adaptive reweighted sampling (CARS) combined with support vector regression (SVR) or random forest (RF) algorithms have demonstrated high accuracy and robustness, with consistent results across ground-based and UAV platforms (Ji et al., 2025; Wu et al., 2025). Machine learning model also significantly outperformed the traditional linear regression model for estimating chlorophyll content. Studies on crops such as winter wheat, corn, and canary have consistently found that algorithms such as RF, SVR, and artificial neural networks (ANNs) provide superior results, with one ANN model for rice achieving very low error rates (Guo et al., 2022; Sarkar et al., 2018). Other studies have also shown a significant positive correlation between soil moisture (SM) and chlorophyll content, suggesting that the VI can serve as an indicator of subsurface conditions (Ge et al., 2019; Wang et al., 2021).

Although the use of remote sensing technology has developed rapidly in monitoring plant physiological conditions, studies on monitoring and estimating soil moisture, leaf water content, and leaf greenness values in oil palm plantations are still relatively limited, especially under conditions of dynamic climate variations, such as precipitation fluctuations. Furthermore, the impact of climate variation on the accuracy of multispectral vegetation index-based estimation models has not been thoroughly studied. Therefore, this study aims to: (1) estimate soil moisture, leaf water content, and leaf greenness from UAV multispectral imagery using machine learning, (2) develop a waterlogging susceptibility classification, and (3) create spatial-temporal waterlogging susceptibility maps.

MATERIAL AND METHODS

Study area

This study was conducted at the Oil Palm Teaching Farm, Cikabayan, IPB University, Bogor, Indonesia (6 °33’ 00.3 “S 106 °43’ 03.2” E), spanning an area of approximately 8 hectares (Figure 1). Oil palm plants were planted in 2011 and have entered the mature phase. The research was carried out from July 2024 to October 2025.

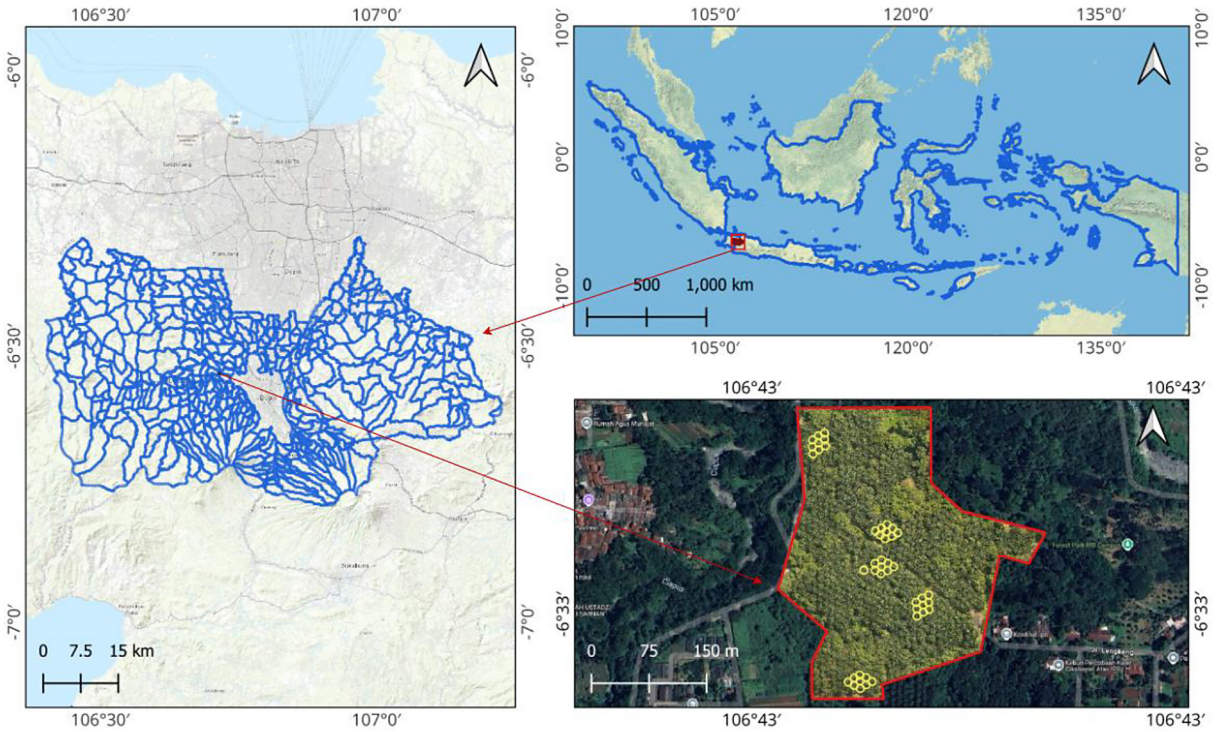

Figure 1. Study area at the Oil Palm Teaching Farm, Cikabayan, IPB University, Bogor, Indonesia

Soil and leaf data collection

A field survey and observational approach were employed, integrating agronomic measurements with multispectral UAV imagery. Field measurements, including soil moisture (SM), leaf water content (LWC), and leaf greenness (LG), were conducted four times: in July 2024, October 2024, January 2025, and April 2025 (Figure 2). A purposive sampling method was employed to select 45 sample plants (representing 5% of the population, as indicated by a yellow circle on the map in Figure 1), chosen to cover a representative range of observed biophysical conditions across the plantation. Soil moisture was determined using the gravimetric method, whereby 50 g of soil samples were collected in triplicate using an auger, weighed for the wet weight, oven-dried at 105 °C for 24 h, and then re-weighed for dry weight. SM was calculated as:

$$SM = \frac{Wet\ weight - \\ - Dry\ weight}{Dry\ weight} \times 100\% \quad (1)$$

The 17th leaf of each sample plant was also analyzed. LWC was determined by collecting leaf samples, recording the fresh weight, cutting leaves into smaller pieces, oven-drying at 80 °C for 48 h to obtain dry weight, and applying the following formula:

$$LWC = \frac{Fresh\ weight - \\ - Dry\ weight}{Fresh\ weight} \times 100\% \quad (2)$$

The LG value was measured directly using a SPAD-502 chlorophyll meter (Konica-Minolta, Japan).

Aerial image acquisition

Aerial image acquisition was performed using a multispectral UAV (DJI Phantom 4 multispectral) at an altitude of 80 m above ground level on four occasions (July 16, 2024, October 16, 2024, January 15, 2025, and April 18, 2025) to represent seasonal variations. All flights were conducted between 09:00 and 11:00 local time under clear-sky conditions. Flight missions were planned using the DJI GS Pro application, which was configured with 75% front overlap and 70% side overlap. Prior to each flight mission, radiometric calibration was performed using a Spectralon calibration reflectance panel (Labsphere, North Sutton, NH, USA). The UAV data processing workflow, from image acquisition to vegetation index extraction, is illustrated in Figure 3.

Figure 2. Soil and leaf samples data collection process

The captured images were processed using Agisoft Metashape Professional software (version 1.8.4) to generate high-resolution outputs, including dense point clouds (in LAS format), digital surface models (DSM, in GeoTIFF format), and orthomosaics (in GeoTIFF format). The orthomosaics were georeferenced to the WGS 84/UTM Zone 48S coordinate system (EPSG:32748). The soil background removal process used spectral index segmentation through the FIELDimageR package in RStudio. Specifically, the HUE index was calculated from the RGB bands and applied as a masking criterion with a threshold value of 0. This approach enables the separation of the vegetation canopy from the ground background by retaining only pixels with HUE index values above the specified threshold, thereby eliminating ground interference from subsequent vegetation analyses.

Individual palm canopies for the 45 sample plants were delineated using the eCognition Oil Palm Application 1.2, and the results were exported as polygon shapefiles. The multispectral orthomosaics were then analyzed in QGIS (version 3.28 'Firenze') to compute 12 vegetation indices using the Raster calculator. Table 1 presents the vegetation indices that were used as predictors. The Zonal Statistics tool was used to extract the mean value of each vegetation index for every delineated canopy, providing a dataset for subsequent predictive modeling of the field-measured parameters (SM, LWC, and LG).

The collected data on SM, LWC, and LG were initially analyzed using descriptive statistics. Pearson's correlation analysis was conducted to examine the basic characteristics and relationships of the data. Subsequently, predictive models were employed using three machine learning algorithms: random forest regression (RFR), partial least squares regression (PLSR), and support vector regression (SVR), with vegetation indices as predictors. Analyses were performed using RStudio version 4.3.2. The dataset was partitioned using the caret package into a 70% training set and a 30% testing set through stratified random sampling, ensuring representative distribution across all seasonal periods. Hyperparameter optimization was conducted automatically via 5-fold cross-validation implemented through the trainControl function in the 'caret' package. RFR models were tuned using the 'randomForest' package with the number of variables randomly sampled at each split (mtry) optimized over the set {2, 3, 5}. PLSR was conducted with the 'pls' package, selecting the optimal number of components (ncomp) from 1 to 10. SVR with a radial basis function kernel was implemented using the 'kernlab' package, where the cost parameter (C) was tuned over {0.1, 1, 10} and the kernel coefficient (sigma) was tuned

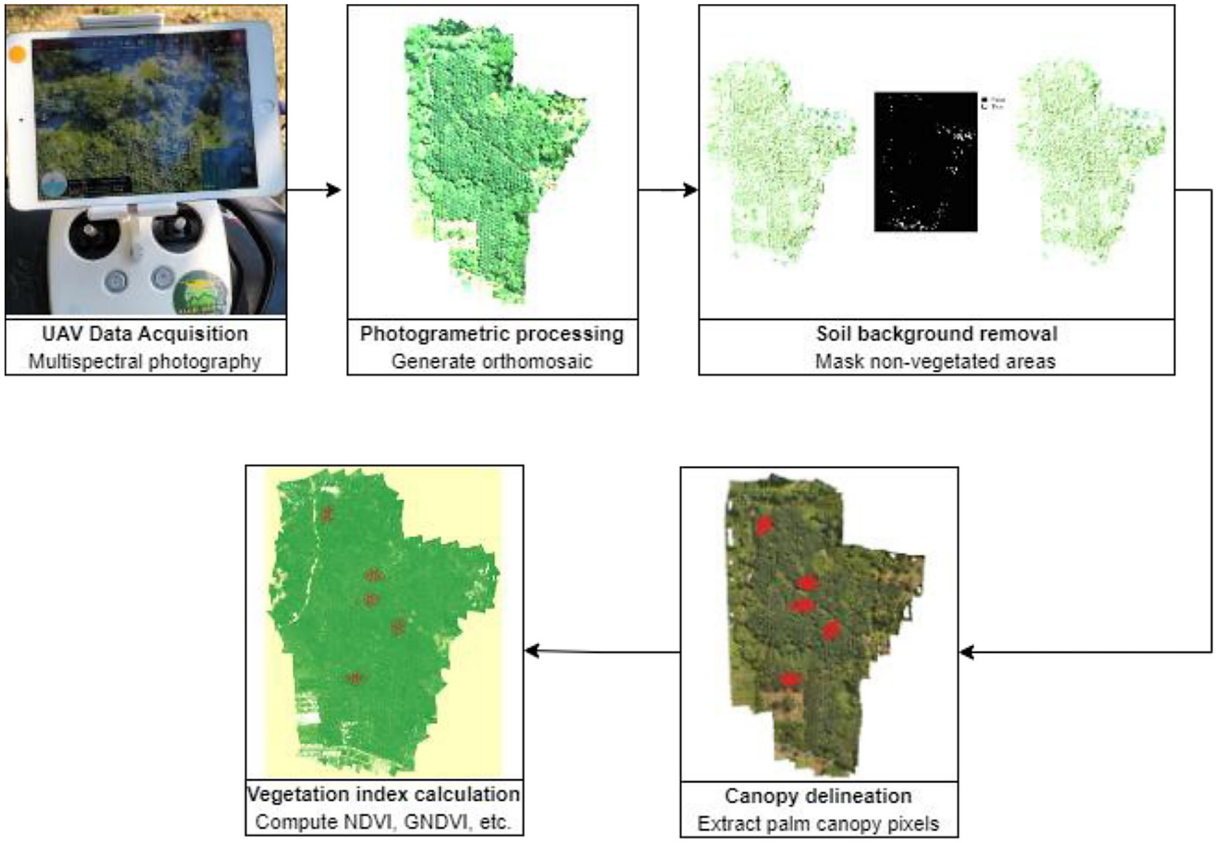

Figure 3. UAV data processing

over {0.01, 0.1, 1}. Data manipulation and visualization were facilitated using the 'dplyr' and 'ggplot2' packages, respectively.

The model performance was evaluated using the coefficient of determination (R^2), root mean squared error (RMSE), and mean absolute error (MAE). These metrics were calculated directly using custom R functions within the RStudio environment, without requiring additional specialized packages. The R^2 values were derived by squaring the Pearson correlation coefficient between the observed and estimated values, whereas the RMSE and MAE were computed using standard mathematical formulas. Higher R^2 values correspond to lower RMSE and MAE values, indicating better model accuracy and estimation precision. Spatial estimation maps for four monitoring periods were generated by applying the best-performing estimation model to all oil palm trees across the plantation. The estimated parameters of water status and leaf greenness were subsequently used for K-means clustering, with the resulting clusters validated against measured fruit production data (black bunch census). Finally, a comprehensive susceptibility assessment map was developed by evaluating the combined frequency of high soil moisture events and depressed leaf greenness values. The three-level susceptibility classification is based on K-means cluster analysis that identifies patterns of relationships between soil moisture, leaf greenness, and productivity, where high susceptibility criteria are applied to plants with soil moisture frequencies above field capacity ≥2 periods and LG <69.21, medium susceptibility for frequencies ≥2 and LG ≥69.21, and low susceptibility for frequencies <2, with the leaf greenness threshold of 69.21 representing the lower limit of productivity that is still acceptable based on field data. The workflow of the research procedure is presented in Figure 4.

RESULT AND DISCUSSION

Descriptive statistics and seasonal variations

Table 2 summarizes the data distribution of the entire dataset, as well as the training and validation subsets, for SM, LWC, and LG parameters. The distribution patterns across observation periods reflected temporal changes in environmental conditions and the physiological responses of

plants. Field measurements in January 2025 exhibited elevated SM and LWC values, with ranges of 47.66–67.93% for SM and 55.71–82.20% for LWC, which were higher than those observed in other periods. Despite these high values, both parameters showed reduced variability during this period, as indicated by lower coefficients of variation and pronounced distribution peaks, suggesting more homogeneous and saturated soil and plant water conditions. The highest SM values recorded in January 2025 indicate persistently humid field conditions, whereas the lowest SM values occurred in July 2024, reflecting comparatively drier conditions. Seasonal changes in SM were consistently mirrored by LWC dynamics, highlighting the close coupling between soil water availability and plant water status. In contrast, LG values remained relatively stable across all observation periods, exhibiting lower variability and near-symmetric distributions, indicating that leaf chlorophyll content was less sensitive to seasonal fluctuations in soil water content.

Table 1. List of vegetation indices

Vegetation indices	References
$NDVI = \frac{NIR - Red}{NIR + Red}$	(Rouse et al., 1974)
$GNDVI = \frac{NIR - Green}{NIR + Green}$	(Gitelson and Merzlyak, 1996)
$SR = \frac{NIR}{Red}$	(Baret and Guyot, 1991)
$MSR = \frac{\left(\frac{\mathrm{NIR}}{\mathrm{Red}}\right) - 1}{\sqrt{\frac{NIR}{Red}} + 1}$	(Chen, 1996)
$NDRE = \frac{NIR - Red\ edge}{NIR + Red\ edge}$	(Haas et al., 1975)
$LCI = \frac{NIR - Red\ edge}{NIR + Red}$	(Zebarth et al., 2002)
$CI_{green} = \frac{NIR}{Green} - 1$	(Gitelson et al., 2005)
$CI_{red\ edge} = \frac{NIR}{Red\ edge} - 1$	(Gitelson et al., 2005)
$RVI = \frac{Red}{NIR}$	(Anderson et al., 1993)
$MPRI = \frac{Green - Red}{Green + Red}$	(Yang et al., 2008)
$EVI = 2.5\frac{NIR - Red}{(NIR + 6\,Red - 7.5\,Blue) + 1}$	(Huete et al., 1999)
$SAVI = 1.5\frac{NIR - Red}{(NIR + Red + 0.5)}$	(Huete, 1988)

Variations in the distribution between observation periods indicated differences in the level of diversity of SM and LWC values, possibly influenced by precipitation dynamics (Figure 5). Meteorological data is available online at URL: https://smpr-geomet.com/dashboard. The highest precipitation intensity occurred from October to December 2024, followed by a decrease in early 2025. The increase in precipitation in late 2024 likely caused higher groundwater accumulation, resulting in increased SM and LWC values during that period, owing to the abundant water availability in the root zone and leaf tissue. Conversely, during the period of low precipitation (January

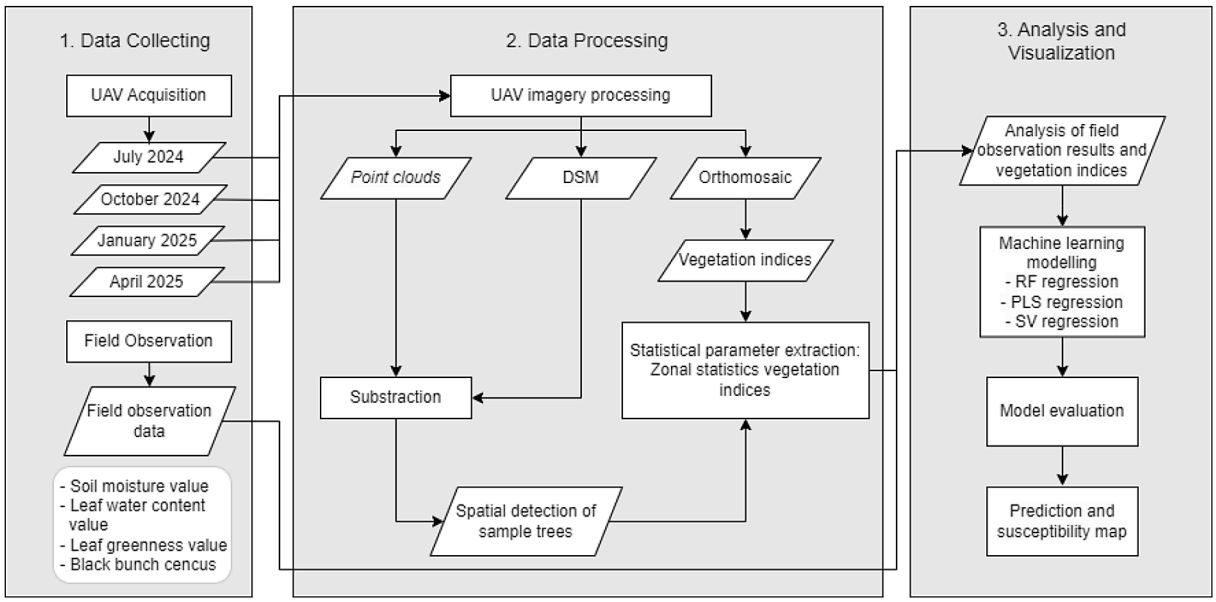

Figure 4. Workflow of waterlogging susceptibility assessment in oil palm plantation

Table 2. Summary statistics of soil moisture, leaf water content, and leaf greenness across four sampling periods (n = 45)

Parameter	Min	Max	Mean	Median	SD	CV	Skewness	Kurtosis
SM July 2024	25.05	51.10	36.72	36.58	6.81	18.60	0.32	2.27
SM October 2024	29.24	57.98	41.10	39.94	6.17	15.00	0.63	3.40
SM January 2025	47.66	67.93	60.54	60.92	3.15	5.20	-1.45	8.07
SM April 2025	29.06	54.49	41.45	42.91	6.25	15.10	-0.22	2.58
LWC July 2024	41.85	53.41	48.88	49.09	2.80	5.70	-0.61	3.17
LWC October 2024	51.70	65.66	56.48	56.42	2.18	3.90	1.40	8.49
LWC January 2025	55.71	82.20	60.76	59.51	4.90	8.10	3.00	12.56
LWC April 2025	48.45	56.98	52.71	52.98	1.80	3.40	-0.16	2.79
LG July 2024	53.03	79.77	70.70	71.43	6.46	9.10	-0.96	3.52
LG October 2024	56.67	91.57	73.21	73.93	7.99	10.90	0.04	2.80
LG January 2025	54.13	81.77	71.60	72.00	5.79	8.10	-0.56	3.42
LG April 2025	59.40	79.69	71.56	72.04	5.38	7.50	-0.38	2.26

Note: SM = soil moisture, LWC = leaf water content, and LG = leaf greenness.

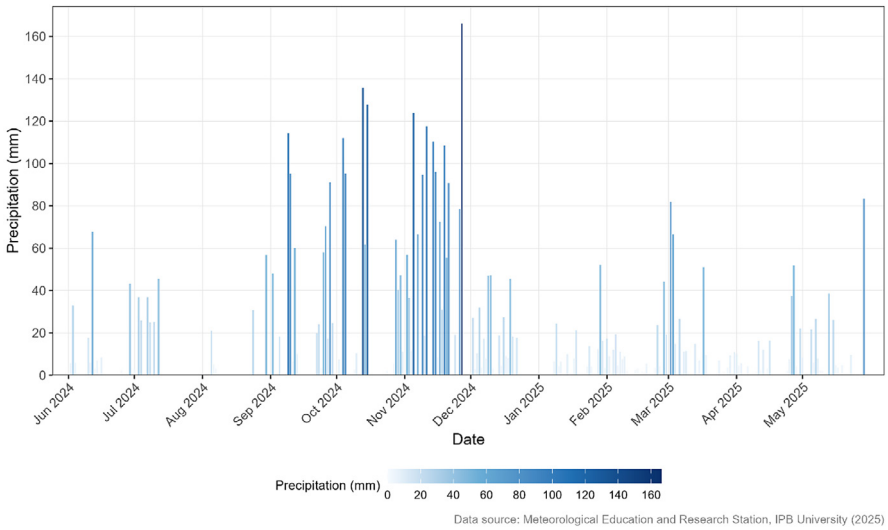

Figure 5. Daily precipitation data during the research period

to April 2025), SM and LWC values decreased, indicating drier soil conditions and reduced leaf water content. In contrast, the LG value was relatively constant between periods compared to SM and LWC, indicating that the chlorophyll content of oil palm leaves was not directly affected by precipitation fluctuations but was more influenced by the plant's internal physiological conditions, which adapted to changes in water availability.

Estimation results using machine learning models

The performances of the SM, LWC, and LG estimation models varied across the observation periods and algorithms (Table 3). The estimation method using multiple vegetation indices as model input variables can increase model accuracy compared to using single vegetation indices (Wu et al., 2023). In general, PLSR demonstrated a more stable performance for predicting SM and LWC, particularly in April 2025, with the highest accuracy (R^2 = 0.613 and R^2 = 0.492, respectively). During periods of high precipitation, such as October 2024, the model performance declined, likely because of the decreased spatial heterogeneity in soil moisture, which affected the consistency of the spectral signal. Leaf water content can be estimated more accurately under conditions with more controlled environmental variability (Alordzinu et al., 2021). In contrast, the relationship between spectral reflectance and leaf tissue water content during

Table 3. Performance of SM, LWC, and LG estimation models on four seasonal variations

Parameter	Period	Model	R^2	RMSE	MAE
SM	July 2024	RFR	0.095	6.114	5.090
SM	July 2024	PLSR	**0.340**	**4.985**	**3.924**
SM	July 2024	SVR	0.195	5.496	4.424
LWC	July 2024	RFR	0.010	3.183	2.575
LWC	July 2024	PLSR	0.015	3.053	2.584
LWC	July 2024	SVR	**0.225**	**3.476**	**2.429**
LG	July 2024	RFR	**0.633**	**4.308**	**3.726**
LG	July 2024	PLSR	0.442	5.036	4.061
LG	July 2024	SVR	0.472	5.263	4.127
SM	October 2024	RFR	0.151	5.619	4.050
SM	October 2024	PLSR	0.307	5.047	3.376
SM	October 2024	SVR	**0.326**	**5.017**	**3.387**
LWC	October 2024	RFR	0.001	3.190	2.315
LWC	October 2024	PLSR	0.022	3.089	2.106
LWC	October 2024	SVR	**0.035**	**3.083**	**2.127**
LG	October 2024	RFR	**0.461**	**8.150**	**6.948**
LG	October 2024	PLSR	0.000	6.931	5.227
LG	October 2024	SVR	0.007	6.492	5.170
SM	January 2025	RFR	0.019	4.843	4.141
SM	January 2025	PLSR	0.001	4.896	4.357
SM	January 2025	SVR	**0.023**	**4.480**	**3.788**
LWC	January 2025	RFR	0.027	3.629	2.601
LWC	January 2025	PLSR	**0.087**	**3.866**	**3.132**
LWC	January 2025	SVR	0.054	3.496	2.365
LG	January 2025	RFR	**0.827**	**5.552**	**4.267**
LG	January 2025	PLSR	0.796	5.919	4.589
LG	January 2025	SVR	0.115	7.068	5.425
SM	April 2025	RFR	0.102	6.295	5.188
SM	April 2025	PLSR	**0.613**	**4.775**	**3.462**
SM	April 2025	SVR	0.277	6.582	5.094
LWC	April 2025	RFR	0.092	2.190	1.792
LWC	April 2025	PLSR	**0.492**	**1.834**	**1.331**
LWC	April 2025	SVR	0.000	2.374	1.884
LG	April 2025	RFR	0.342	4.927	3.975
LG	April 2025	PLSR	**0.500**	**4.470**	**3.676**
LG	April 2025	SVR	0.332	5.104	4.337

Note: SM = soil moisture, LWC = leaf water content, LG = leaf greenness.

wet periods becomes more complex (Yang et al., 2023). These results confirm that the influence of atmospheric conditions and leaf surface water content must be considered in multispectral data-based modeling. RFR provided the best results for LG estimation, particularly in January 2025, indicating the model's ability to better capture variations in chlorophyll content (R^2 = 0.827). The differences in model performance between periods reflect the influence of seasonal environmental conditions on spectral relationships and physiological variables, as reported by Ismail et al. (2025), that seasonal fluctuations in vegetation health also determine the strength of spectral relationships, where wetter periods produce more accurate estimation. Both models were also robust to data containing multicollinearity (Li et al., 2025). Differences in the capabilities of algorithm models are a consideration

when selecting multispectral data-based models, particularly under the influence of atmospheric conditions and leaf surface water content (Qu et al., 2024; Tang et al., 2022).

To further elucidate the underlying relationships driving these model performances, a detailed correlation analysis was conducted between the measured parameters and various vegetation indices. Based on Pearson's correlation heatmap (Figure 6), SM consistently showed a negative correlation with most vegetation indices, except for the RVI. The negative correlation was particularly strong with SR and MSR in July 2024, October 2024, and April 2025, when soil moisture conditions were not particularly high. This indicates that increasing soil moisture decreases the reflectance in the NIR and red bands, which are sensitive to canopy water content. Conversely, LWC showed a weak and inconsistent correlation, indicating that leaf water content is more influenced by internal physiological factors and atmospheric conditions than by spectral variation. LG exhibited a pattern similar to that of SM but with positive correlations with some vegetation indices throughout the observation period. The strongest correlations were observed with red-edge-based indices, such as NDRE, LCI, and CIrededge, in October 2024, January 2025, and April 2025. These results demonstrate the advantage of red edge reflectance for detecting variations in leaf chlorophyll content, as stated by Ali et al. (2022), who reported that the red edge position (REP) is strongly correlated with chlorophyll content. Red-edge light can penetrate much further into the leaf than blue or red light (Parida et al., 2024). The relationship pattern confirms that water-related variables (SM and LWC) are more influenced by precipitation dynamics, whereas LG is more stable and can be well explained by changes in vegetation reflectance.

Best-performing models

Figure 7 presents the relationship between the actual and estimated values based on the best models identified previously. The PLSR model demonstrated relatively high accuracy in predicting soil moisture in April 2025 ($R^2 = 0.613$), indicating its ability to capture a strong linear relationship between reflectance and soil water content. Weaker estimations in January 2025 suggest reduced spectral sensitivity to soil moisture variations under wet conditions. For LWC, all models

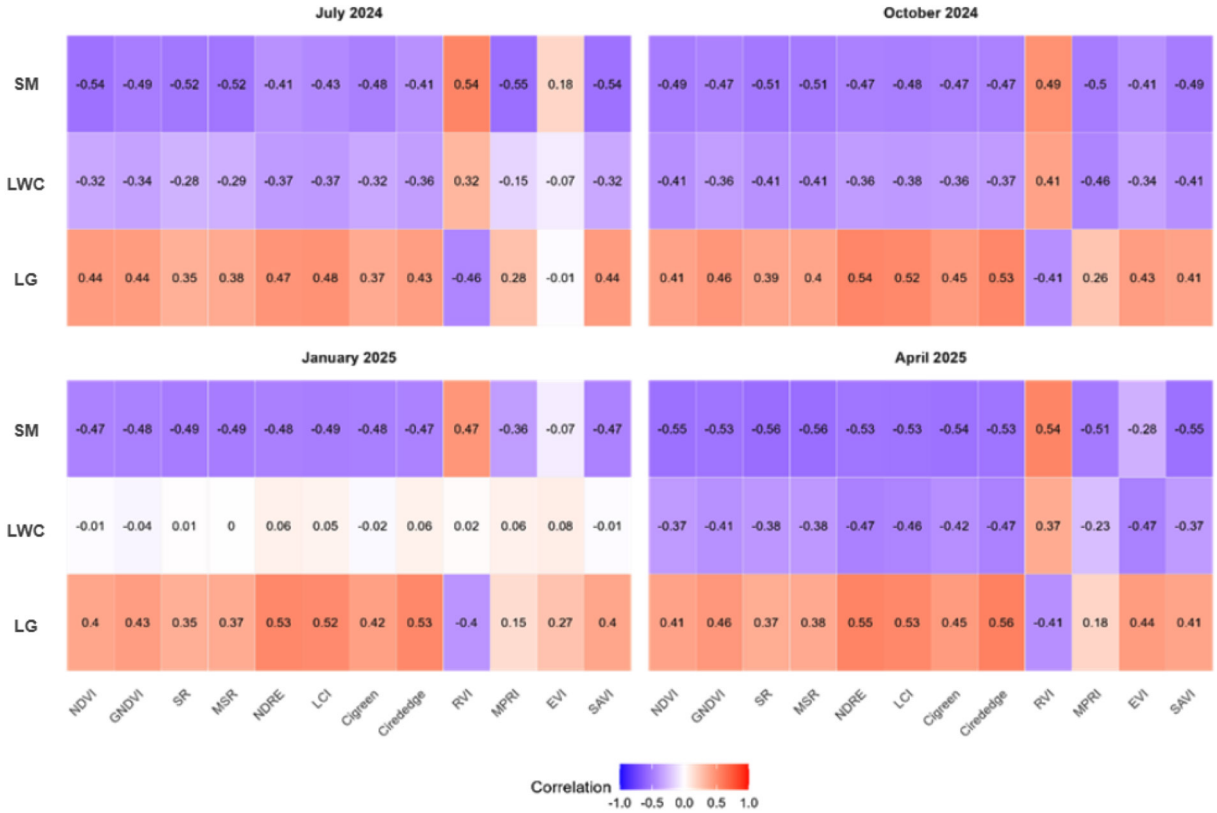

Figure 6. Comparison of performance metrics of different models for predicting SM, LWC, and LG

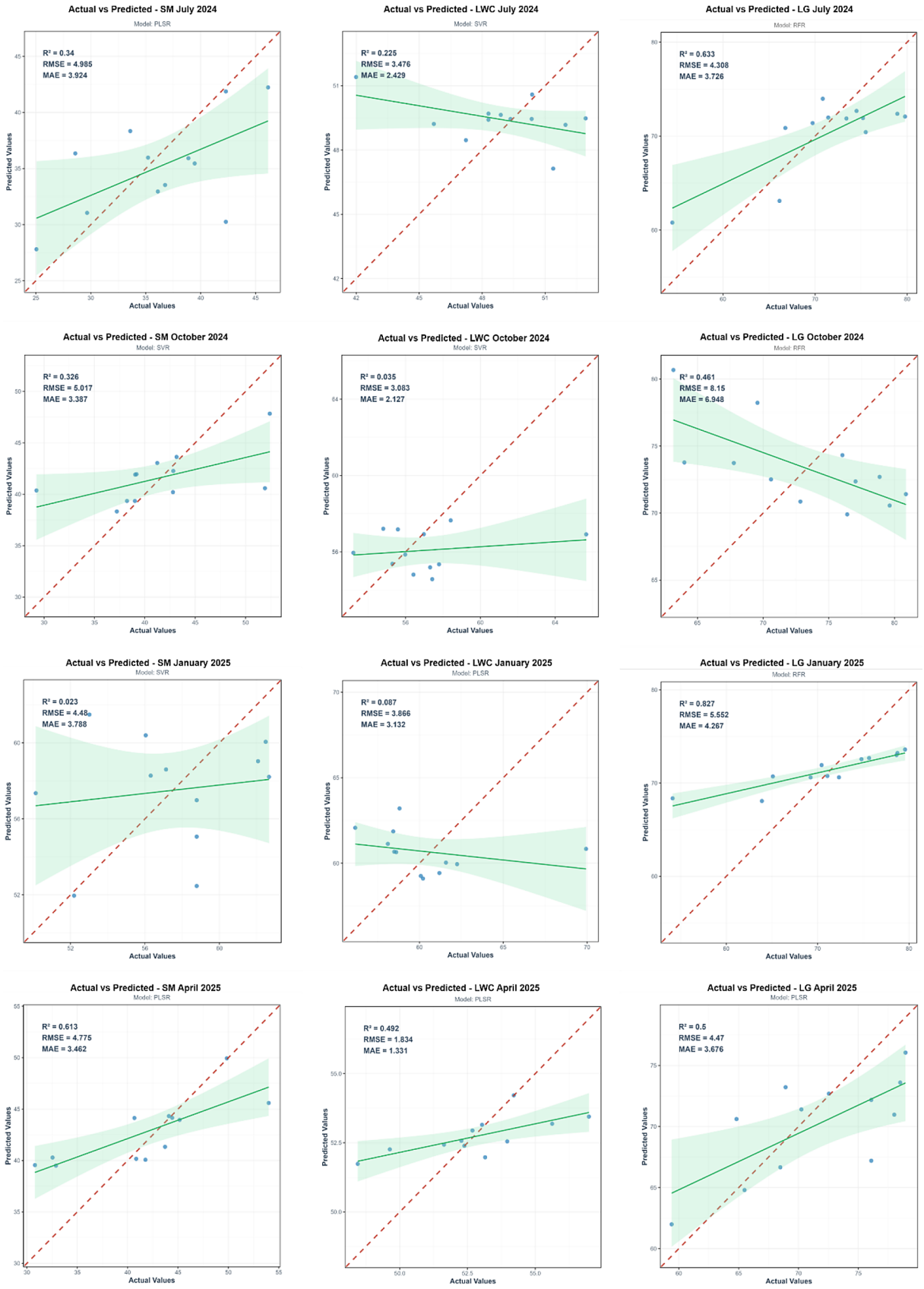

Figure 7. Actual vs estimated values of SM, LWC, and LG from the best model

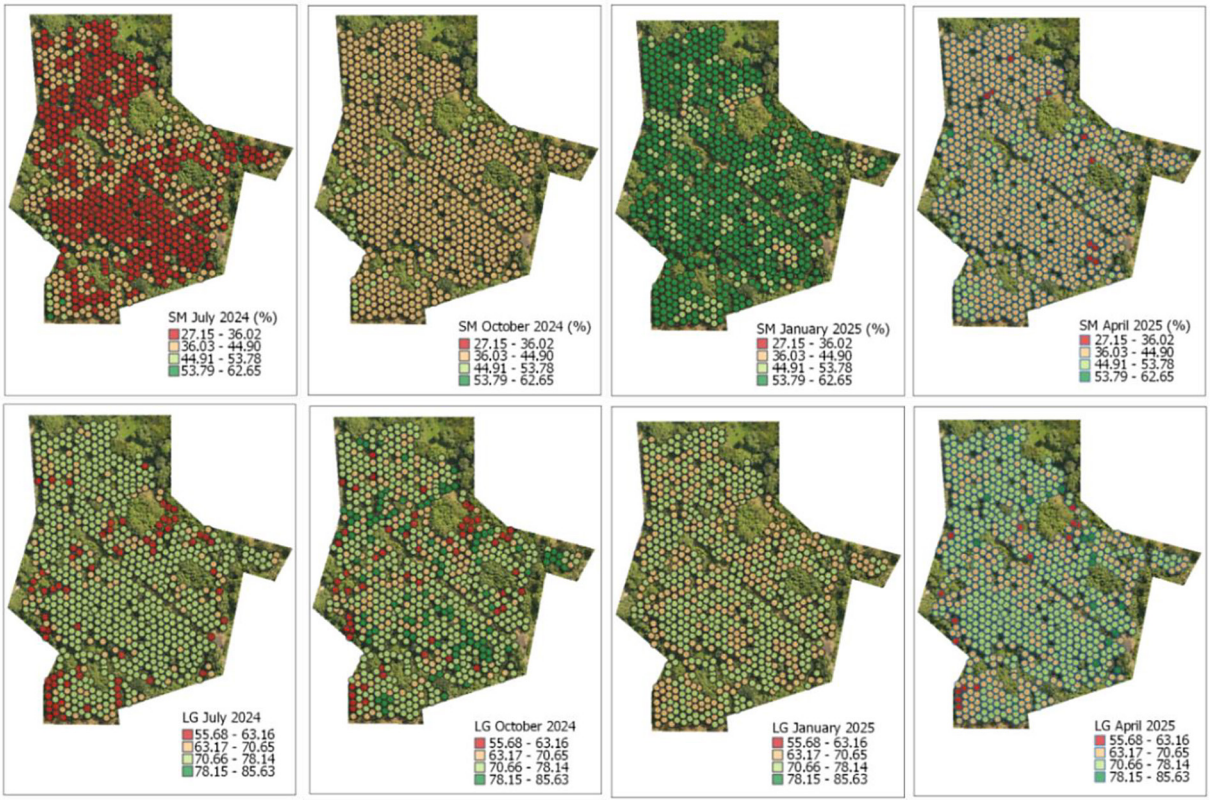

Figure 8. Estimation map generated based on the best model

exhibited a weak relationship, with low R^2 values, reflecting the limited wavelengths available for the accurate detection of variations in leaf water content. For LG, the estimation models consistently performed best, particularly the RFR and PLSR models in January and April, demonstrating a high level of agreement between the actual and estimated values ($R^2 > 0.79$). The RFR model appears to better capture nonlinear patterns between variables and is more adaptable to data complexity, whereas PLSR has advantages in terms of stability and easier interpretation of linear relationships. These two models complement each other in modeling oil palm physiological parameters based on multispectral data.

The spatial estimation maps generated from the best-performing models demonstrated the practical potential of integrating multispectral UAV data into precision agriculture workflows (Figure 8). Due to its low predictive validity, the estimation of leaf water content was excluded from subsequent analysis. To assess waterlogging susceptibility, we analyzed the frequency of elevated soil moisture events, using the soil's field capacity (39%) as a critical threshold for excess moisture, as established by Jazayeri et al. (2015). A corresponding critical threshold for leaf greenness value of 67.71 was determined empirically from the K-means clustering results. This value represents the midpoint between the maximum leaf greenness value observed in the lowest-productivity cluster (Cluster 1) and the minimum leaf greenness value in the intermediate-productivity cluster (Cluster 2), as shown in Figure 9a. The integration of this biophysical clustering with yield estimation from black bunch census confirmed that palm clusters exhibiting consistently high soil moisture (exceeding field capacity) concurrently with low leaf greenness (below the critical threshold) were associated with the lowest agricultural productivity (Figure 9b). This synthesized susceptibility assessment was subsequently used to generate a spatial map of waterlogging susceptibility for the plantation (Figure 9c).

The spatial waterlogging susceptibility map (Figure 9c) indicates that high susceptibility palms (red; 10.13%) are concentrated in areas with compacted soils and poor drainage function. Medium susceptibility palms (yellow; 77.18%) generally occupy areas with moderate soil wetness, including several depressional sections observed in the field, while low susceptibility palms (green, 12.69%) are distributed across well-drained portions of the plantation. These spatial patterns are

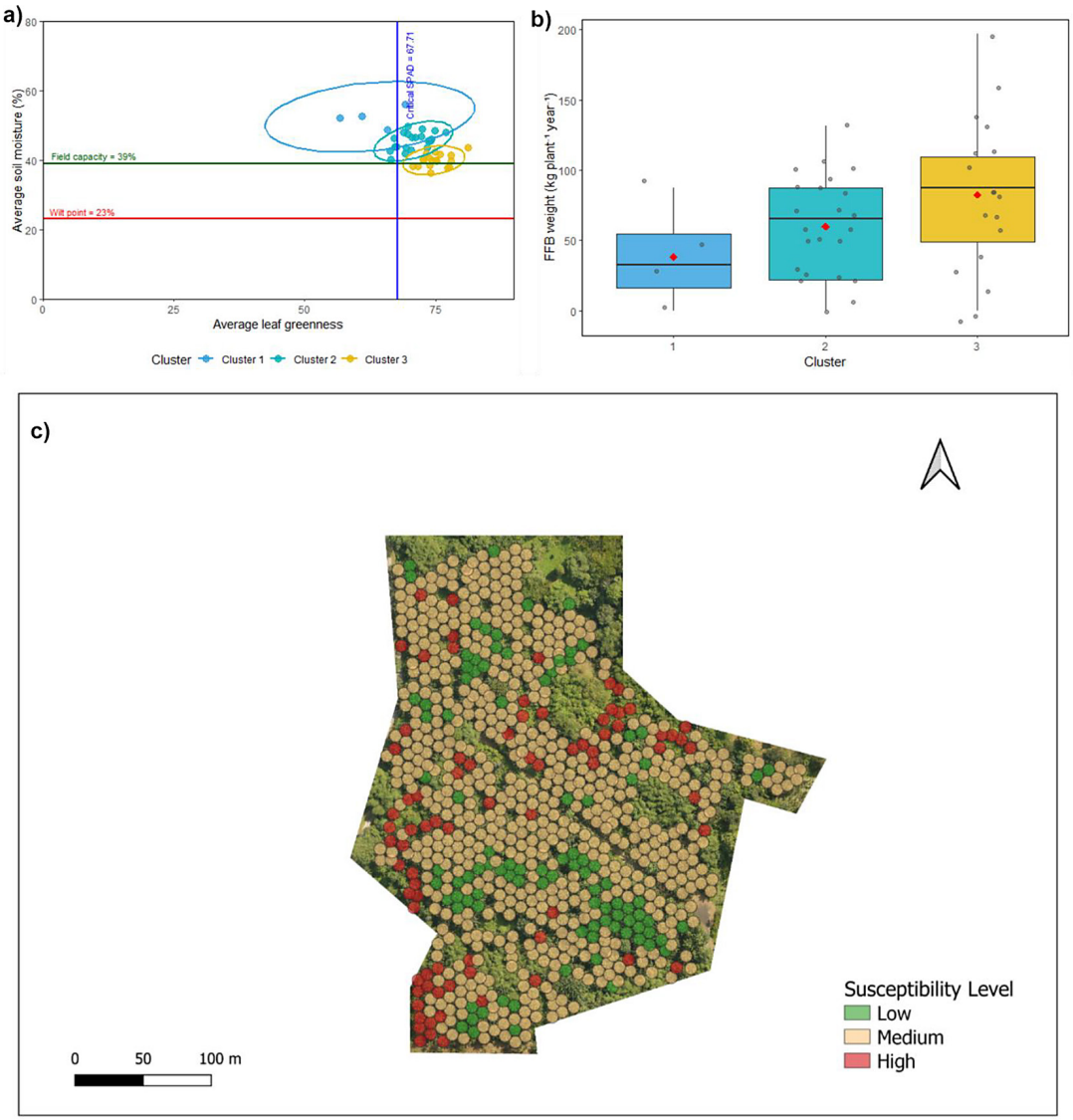

Figure 9. Clustering of oil palm trees based on average values of soil moisture and leaf greenness (a), distribution of annual fresh fruit bunch yield across clusters used for validation (b), and spatial distribution of waterlogging susceptibility levels (c)

further intensified by the high precipitation characteristics of Bogor Regency, which is known as one of the wettest regions in Indonesia, receiving approximately 2.961–4.266 mm of annual precipitation (Wardani et al., 2024). Such precipitation conditions increase the likelihood of prolonged soil saturation, especially in areas with limited infiltration or inadequate drainage. These conditions create a challenging environment for palm growth, as prolonged waterlogging can lead to root oxygen deficiency and increased susceptibility to diseases (den Besten et al., 2021; Walne and Reddy, 2021). Effective drainage management is therefore critical to mitigate this susceptibility and sustain plantation productivity. Implementing site-specific interventions, such as soil aeration or constructing drainage channels, can help mitigate the impacts of waterlogging in vulnerable zones (Abubakar et al., 2021).

By estimating the spatial dynamics of crop and soil biophysical parameters, these models can support site-specific management practices. In the future, this approach will provide a scalable framework for real-time crop monitoring, enabling oil palm plantation management to make data-driven decisions that improve resource efficiency and resilience under varying hydrological conditions. UAV-based remote sensing has strong potential for operational applications in plantation management, offering a rapid, non-destructive, and cost-effective method for assessing plant health and productivity in oil palm cultivation.

CONCLUSIONS

This study demonstrates the potential of using UAV-based multispectral imagery combined with three machine learning algorithms to estimate water status and physiological parameters in oil palm plantations under varying seasonal conditions. Seasonal dynamics influence the relationship between spectral responses and physiological variables. The PLSR model provided the best accuracy for soil moisture estimation, while RFR and PLSR showed the highest performance for estimating leaf greenness values. The accuracy of the leaf water content model was relatively low, indicating limited spectral sensitivity to variations in leaf water content in dense oil palm canopies. The results of this study emphasize the importance of selecting a predictive modeling approach that is tailored to the biophysical characteristics of the target variables and the seasonally fluctuating field conditions. These findings showed that multispectral UAV imagery can provide reliable estimates of leaf greenness and soil moisture. The spatial estimates of soil moisture and leaf greenness derived from multispectral UAV imagery further enabled the identification of palms susceptible to waterlogging stress. These spatial susceptibility assessments offer a practical approach to mitigation and support more informed decision-making for precision management in oil palm plantations.

REFERENCES

1. Abubakar, A., Ishak, M. Y., Makmom, A. A. (2021). Impacts of and adaptation to climate change on the oil palm in Malaysia: A systematic review. *Environmental Science and Pollution Research*, *28*(39), 54339–54361. https://doi.org/10.1007/s11356-021-15890-3
2. Ali, A., Imran, M., Ali, A., Khan, M. A. (2022). Evaluating Sentinel-2 red edge through hyperspectral profiles for monitoring LAI & chlorophyll content of Kinnow Mandarin orchards. *Remote Sensing Applications: Society and Environment*, *26*, 100719. https://doi.org/10.1016/j.rsase.2022.100719
3. Alordzinu, K. E., Li, J., Lan, Y., Appiah, S. A., AL Aasmi, A., Wang, H., Liao, J., Sam-Amoah, L. K., Qiao, S. (2021). Ground-based hyperspectral remote sensing for estimating water stress in tomato growth in sandy loam and silty loam soils. *Sensors*, *21*, 5705. https://doi.org/10.3390/s21175705
4. Anderson, G. L., Hanson, J. D., Haas, R. H. (1993). Evaluating landsat thematic mapper derived vegetation indices for estimating above-ground biomass on semiarid rangelands. *Remote Sensing of Environment*, *45*(2), 165–175. https://doi.org/10.1016/0034-4257(93)90040-5
5. Baret, F., Guyot, G. (1991). Potentials and limits of vegetation indices for LAI and APAR assessment. *Remote Sens. Environ*, *35*, 161–173. https://doi.org/https://doi.org/10.1029/2005GL022688
6. Chen, J. M. (1996). Evaluation of vegetation indices and a modified simple ratio for boreal applications. *Canadian Journal of Remote Sensing*, *22*(3), 229–242. https://doi.org/10.1080/07038992.1996.10855178
7. den Besten, N., Steele-Dunne, S., de Jeu, R., van der Zaag, P. (2021). Towards monitoring waterlogging with remote sensing for sustainable irrigated agriculture. *Remote Sensing*, *13*(15), 2929. https://doi.org/10.3390/rs13152929
8. Falcioni, R., Santos, G. L. A. A. dos, Crusiol, L. G. T., Antunes, W. C., Chicati, M. L., Oliveira, R. B. de, Demattê, J. A. M., Nanni, M. R. (2023). Non−invasive assessment, classification, and prediction of biophysical parameters using reflectance hyperspectroscopy. *Plants*, *12*, 2526. https://doi.org/10.3390/plants12132526
9. Ge, X., Wang, J., Ding, J., Cao, X., Zhang, Z., Liu, J., Li, X. (2019). Combining UAV-based hyperspectral imagery and machine learning algorithms for soil moisture content monitoring. *PeerJ*, *7*, e6926. https://doi.org/10.7717/peerj.6926
10. Gitelson, A. A., Merzlyak, M. N. (1996). Signature analysis of leaf reflectance spectra: Algorithm development for remote sensing of chlorophyll. *Journal of Plant Physiology*, *148*(3–4), 494–500. https://doi.org/https://doi.org/10.1016/S0176-1617(96)80284-7
11. Gitelson, A. A., Viña, A., Ciganda, V., Rundquist, D. C., Arkebauer, T. J. (2005). Remote estimation of canopy chlorophyll in crops. *Geophysical Research Letters*, *32*(8).
12. Guo, Y., Chen, S., Li, X., Cunha, M., Jayavelu, S., Cammarano, D., Fu, Y. (2022). Machine learning-based approaches for predicting SPAD values of maize using multi-spectral images. *Remote Sensing*, *14*, 1337.
13. Haas, R. H., Deering, D. W., Rouse, J. W., Schell, J. A. (1975). Monitoring vegetation conditions from Landsat for use in range management. *NASA Earth Resources Survey Symposium Proc.*, 43–52.
14. Huete, A. (1988). A soil-adjusted vegetation index (SAVI). *Remote Sensing of Environment*, *25*(3), 295–309. https://doi.org/10.1016/0034-4257(88)90106-X
15. Huete, A., Justice, C., Van Leeuwen, W. (1999). *MODIS vegetation index (MOD13)* (p. 125371817).
16. Jackson, T. A., Crawford, J. W., Traeholt, C., Sanders, T. A. B. (2019). Learning to love the world's most hated crop. *Journal of Oil Palm Research*, *31*(3), 331–347. https://doi.org/10.21894/jopr.2019.0046

17. Jazayeri, S. M., Rivera, Y. D., Camperos-Reyes, J. E., Romero, H. M. (2015). Physiological effects of water deficit on two oil palm (*Elaeis guineensis* Jacq.) genotypes. *Agronomia Colombiana*, *33*(2), 164–173. https://doi.org/10.15446/agron.colomb.v33n2.49846
18. Jha, G., Debangshi, U., Palla, S., Nazrul, F., Dey, S., Dutta, W., Bansal, S. (2025). Precision Agriculture Technologies for Climate-Resiliency and Water Resource Management. In: A. Nanda, P. K. Gupta, V. Gupta, P. K. Jha, & S. K. Dubey (Eds.), *Navigating the Nexus* 351–381. Springer, Cham. https://doi.org/10.1007/978-3-031-76532-2_15
19. Ji, J., Lu, X., Ma, H., Jin, X., Jiang, S., Cui, H., Lu, X., Yang, Y. (2025). Estimation of plant leaf water content based on spectroscopy. *Frontiers in Plant Science*, *16*, 1609650. https://doi.org/10.3389/fpls.2025.1609650
20. Khor, J. F., Ling, L., Yusop, Z., Tan, W. L., Ling, J. L., Soo, E. Z. X. (2021). Impact of el niño on oil palm yield in malaysia. *Agronomy*, *11*, 2189. https://doi.org/10.3390/agronomy11112189
21. Li, M., Wang, W., Li, H., Yang, Z., Li, J. (2025). Monitoring of vegetation chlorophyll content in photovoltaic areas using UAV-mounted multispectral imaging. *Frontiers in Plant Science*, *16*, 1643945. https://doi.org/10.3389/fpls.2025.1643945
22. Malike, F. A., Shamsudin, N. A. A., Amiruddin, M. D., Marjuni, M., Yaakub, Z. (2024). Development of new high-yielding planting material based on performance of 38 oil palm (*Elaeis guineensis* Jacq.) Dura × Pisifera families. *Euphytica*, *220*(5), 73. https://doi.org/https://doi.org/10.1007/s10681-024-03333-2
23. Murphy, D. J., Goggin, K., Paterson, R. R. M. (2021). Oil palm in the 2020s and beyond: challenges and solutions. *CABI Agriculture and Bioscience*, *2*, 39. https://doi.org/10.1186/s43170-021-00058-3
24. Parida, P. K., Somasundaram, E., Krishnan, R., Radhamani, S., Sivakumar, U., Parameswari, E., Raja, R., Shri Rangasami, S. R., Sangeetha, S. P., Gangai Selvi, R. (2024). Unmanned aerial vehicle-measured multispectral vegetation indices for predicting LAI, SPAD chlorophyll, and yield of maize. *Agriculture (Switzerland)*, *14*, 1110. https://doi.org/10.3390/agriculture14071110
25. Qu, T., Li, Y., Zhao, Q., Yin, Y., Wang, Y., Li, F., Zhang, W. (2024). Drone-based multispectral remote sensing inversion for typical crop soil moisture under dry farming conditions. *Agriculture*, *14*(3), 484. https://doi.org/10.3390/agriculture14030484
26. Rauf, S. (2025). Status of various sources of edible oil and prospects of oil palm cultivation in Pakistan. *OCL*, *32*, 30. https://doi.org/10.1051/ocl/2025028
27. Rouse, J. W., Haas, R. H., Schell, J. A., Deering, D. W. (1974). Monitoring vegetation systems in the Great Okains with ERTS. *The Third Earth Resources Technology Satellite—1 Symposium*, 309–317.
28. Sarkar, T. K., Ryu, C., Kang, J., Kang, Y., Jun, S., Jang, S., Park, J., Song, H. (2018). Artificial neural network-based model for predicting moisture content in rice using UAV remote sensing data. *Korean Journal of Remote Sensing*, *34*(4), 611–624.
29. Tang, Z., Jin, Y., Alsina, M. M., McElrone, A. J., Bambach, N., Kustas, W. P. (2022). Vine water status mapping with multispectral UAV imagery and machine learning. *Irrigation Science*, *40*, 715–730. https://doi.org/10.1007/s00271-022-00788-w
30. Walne, C. H., Reddy, K. R. (2021). Developing functional relationships between soil waterlogging and corn shoot and root growth and development. *Plants*, *10*, 2095.
31. Wang, J., Zhou, Q., Shang, J., Liu, C., Zhuang, T., Ding, J., Xian, Y., Zhao, L., Wang, W., Zhou, G., Tan, C., Huo, Z. (2021). UAV- and machine learning-based retrieval of wheat SPAD values at the overwintering stage for variety screening. *Remote Sensing*, *13*, 5166.
32. Wardani, I. K., Puteri, D. W., Musyarofah, N., Darmawan, M. (2024). Mapping climate suitability for oil palm using geographical information system in Bogor Regency. *IOP Conference Series: Earth and Environmental Science*, 1–10. https://doi.org/10.1088/1755-1315/1386/1/012028
33. Wu, Q., Zhang, Y., Zhao, Z., Xie, M., Hou, D. (2023). Estimation of relative chlorophyll content in spring wheat based on multi-temporal UAV remote sensing. *Agronomy*, *13*, 211.
34. Wu, Y., Yuan, S., Zhu, J., Tang, Y., Tang, L. (2025). Estimation of wheat leaf water content based on UAV hyper-spectral remote sensing and machine learning. *Agriculture*, *15*, 1898.
35. Yang, B., Zhang, H., Lu, X., Wan, H., Zhang, Y., Zhang, J., Jin, Z. (2023). Inversion of leaf water content of Cinnamomum camphora based on preferred spectral index and machine learning algorithm. *Forests*, *14*, 2285. https://doi.org/10.3390/f14122285
36. Yang, Z., Willis, P., Mueller, R. (2008). Impact of band-ratio enhanced AWIFS image to crop classification accuracy. *Pecora 17 – The Future of Land Imaging…Going Operational*, 11.
37. Zebarth, B. J., Younie, M., Paul, J. W., Bittman, S. (2002). Evaluation of leaf chlorophyll index for making fertilizer nitrogen recommendations for silage corn in a high fertility environment. *Communications in Soil Science and Plant Analysis*, *33*, 665–684. https://doi.org/10.1081/CSS-120003058
38. Zeng, Y., Hao, D., Huete, A., Dechant, B., Berry, J., Chen, J. M., Joiner, J., Frankenberg, C., Bond-Lamberty, B., Ryu, Y., Xiao, J., Asrar, G. R., Chen, M. (2022). Optical vegetation indices for monitoring terrestrial ecosystems globally. *Nature Reviews Earth & Environment*, *3*(7), 477–493. https://doi.org/10.1038/s43017-022-00298-5